Progress In Electromagnetics Research M, Vol. 87, 53–62, 2019

Radiation from Reflector Antenna of Finite Thickness and Conductivity in Resonant Scattering Band

Oleg Sukharevsky[1, *], Sergey Nechitaylo[1], Valery Orlenko[1], Vitaly Vasylets[1], and Serhy Fryz[2]

Abstract—A method is proposed for calculating the radiation characteristics of a reflector antenna in the resonant wavelength range. The method uses the solution of the problem of electromagnetic field scattering from a well-conducting non-closed screen of finite thickness. This problem is solved by an E-field integral equation and on approximate boundary conditions by Leontovich, which are applied onto a surface of a well-conducting screen.

1. INTRODUCTION

Many applied problems in the theory of reflector antennas involve the need to know the antenna radiation characteristics in the range of wavelengths, which are resonant with respect to the size of its reflector. In particular, such a task may arise when transmitting (receiving) antennas are designed for ultra-wideband (UWB) signals given that the entire spectrum of the signal falls within the specified range. In this case, the well-known methods of short-wave diffraction [1] cannot be applied. When calculating the radiation characteristics of such antennas, the problem of electromagnetic waves scattering from conductive non-closed thin screens of resonant sizes needs to be solved.

In a number of works [2–13], this problem has been solved under assumptions of infinitely thin and perfectly conducting screens. However, as shown in [14], in resonant wave scattering band ($k_0 b \sim 10$, where k_0 is the wavenumber in free space, and b is the characteristic size of the screen described by the radius of the reflector's aperture), such an assumption can lead to great errors.

In works [15, 16], the problem of wave scattering from the finite thickness screens was solved by means of E-field integral equation. Singularity of an equation kernel was eliminated by shifting boundary conditions from the screen surface onto an auxiliary surface within the screen as in [17, 18]. Nevertheless, in [15, 16], the scattering characteristics were calculated under the assumption of perfectly conducting screens. However, elements of real antennas are made of materials with great but finite conductivity. Conductivity of metals and alloys that reflectors are made of can vary in a wide range. For instance, conductivity of aluminum is 3.54×10^7 Sm/m, and that of duralumin 2024 (alloy of Al-Cu-Mg) is 1.74×10^7 Sm/m.

However, in the known works, the study of scattering from thin (but not zero thin) screens having great (but not perfect) conductivity was not carried out.

Nevertheless, development of the method for computing the scattering characteristics of the structures mentioned here was not our only purpose. We propose a method of numerical implementation to apply a computation of impulse responses of reflector antennas including thin (but not zero thin) screens having great (but not infinite) conductivity.

Received 4 September 2019, Accepted 19 November 2019, Scheduled 4 December 2019

* Corresponding author: Oleg Sukharevsky (sukharevsky@euro.dinos.net).

[1] Kharkiv National Ivan Kozhedub University of Air Forces, 77/79 Sumska street, Kharkiv 61023, Ukraine. [2] Zhytomyr Military Institute, 22 Myru av., Zhytomyr 10004, Ukraine.

So, this paper presents a generalization of the E-field integral equation onto the case of non-perfectly conducting screens of finite thickness. Besides, we obtain a system of integral equations (SIE) that utilizes impedance boundary conditions at the screen's surface. We present an example of employing SIE for evaluating radiating properties of reflector antenna with regard to UWB signals.

2. PROBLEM FORMULATION

Let's suppose that a well-conducting object V (Fig. 1) is placed into an infinite homogeneous isotropic medium with permittivity ε_0 and permeability μ_0. Let S be the surface of object V.

Electromagnetic field at point M can be expressed as

$$\vec{E}(M) = \vec{E}^0(M) + \vec{E}^s(M),$$
$$\vec{H}(M) = \vec{H}^0(M) + \vec{H}^s(M),$$

where $\vec{E}^s(M)$, $\vec{H}^s(M)$ is the scattered electromagnetic field, and $\vec{E}^0(M)$, $\vec{H}^0(M)$ is the incident electromagnetic field.

Our objective is to find the field $\vec{E}^s(M)$, $\vec{H}^s(M)$ scattered by the object.

We use the integral representation of electromagnetic field at point M (Fig. 1) with respect to electric field intensity $\vec{E}$ [19, 20]

$$\vec{E}(M) = \vec{E}^0(M) - \oint\limits_S j\omega\mu_0 g(r)\vec{J}ds_p - \oint\limits_S \left\{\left(\left(\vec{n}_p \times \vec{E}\right) \times \vec{\nabla} g(r)\right) + \left(\vec{n}_p \cdot \vec{E}\right)\vec{\nabla} g(r)\right\} ds_p, \quad (1)$$

where $g(r) = \frac{1}{4\pi}\frac{e^{jk_0 r}}{r}$; r is the distance from observation point M to point P, the latter sitting at the surface S (Fig. 1); $\vec{n}_p$ is the unit vector of internal normal to the surface S at point P; $\vec{J}(P) = \vec{n}_p \times \vec{H}$ is the surface current density at point P.

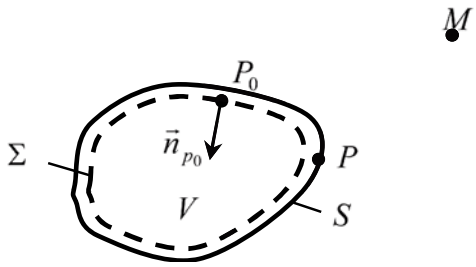

Figure 1. Geometry of the problem.

The field dependence upon time is assumed to have the form of $e^{-j\omega t}$.

Now, we suppose that the Leontovich approximate boundary condition holds at the surface S [21]:

$$\vec{n}_p \times \vec{E} = W\left(\vec{n}_p \times \vec{J}\right) \text{ at } S, \quad (2)$$

where $W = \sqrt{\frac{\mu_0}{\varepsilon_0}}Z = \sqrt{\frac{\mu_a}{\varepsilon_a}}$ is the surface impedance of the boundary surface S; ε_a is the permittivity; and μ_a is the permeability of material that object V is made of.

Substituting expression (2) into (1), we receive integral representation for electromagnetic field scattered by the impedance object V:

$$\vec{E}(M) = \vec{E}^0(M) - \oint\limits_S j\omega\mu_0 g(r)\vec{J}ds_p - \oint\limits_S \left\{W\left(\left(\vec{n}_p \times \vec{J}\right) \times \vec{\nabla} g(r)\right) + \left(\vec{n}_p \cdot \vec{E}\right)\vec{\nabla} g(r)\right\} ds_p. \quad (3)$$

In the problem at hand, object V is a metallic one with non-perfect conductivity. Depth of the wave penetration into metal is described by the depth of skin layer $\Delta_0 = \sqrt{\frac{2}{\omega\mu_0\mu\sigma}}$ [21]. At high frequencies,

this penetration depth is small enough, and we can assume that at the depths significantly exceeding this skin layer depth there will be no electromagnetic field inside the metal. This gives us grounds to apply the null-field method [22–24] to the form in Eq. (3). We introduce an auxiliary surface Σ within V. This surface is placed at the depth Δ under the surface S, with the distance Δ being much greater than the skin layer depth and the shape of Σ repeating that of S. In our computations, we set Δ equal to $10\Delta_0$, which corresponds to wave attenuation by the factor of e^{10}. We have also repeated calculations given other values of Δ, particularly $8\Delta_0$ and $12\Delta_0$, and the computational results deviate by not more than 0.8%.

Let's now move observation point M to a point P_0 that sits at the surface Σ (Fig. 1). Then, let's suppose that total field $\vec{E}(P_0)$ at point P_0 at the surface Σ would be equal to zero.

After some transformations of formula (3), we obtain the vector-integral equation of the first kind:

$$\vec{E}^0(P_0) = \oint\limits_S j\omega\mu_0 g(r)\,\vec{J}\,ds_p + \oint\limits_S \left\{W\left(\left(\vec{n}_p \times \vec{J}\right) \times \vec{\nabla} g(r)\right) + E_n(P)\,\vec{\nabla} g(r)\right\} ds_p,\ P_0 \in \Sigma. \tag{4}$$

In Equation (4), the surface current density $\vec{J}(P)$ and normal component of electric field $E_n(P) = \vec{n}_p \cdot \vec{E}(P)$ at point P of surface S are unknowns.

Now, the integral in the right-hand part of Equation (4) becomes non-singular one. The latter is because the observation point P_0 and source point P are now situated at different surfaces. The latter simplifies numerical integration of Equation (4).

Now, we multiply Equation (4) by $\vec{n}_{p_0}$ (the unit vector of internal normal to surface Σ at point P_0) on the right, and we multiply it twice, the first product being the vector one and the second being the scalar one (dot product). In this manner, we get the following SIE [25, 26]:

$$\begin{aligned}
&\oint\limits_S \left\{j\omega\mu_0 g(r)\left(\vec{n}_{p_0} \times \vec{J}\right) + \left(\vec{n}_{p_0} \times \vec{\nabla} g(r)\right) E_n(P)\right. \\
&\left. + W\left[\left(\vec{n}_{p_0} \times \vec{J}\right)\left(\vec{\nabla} g(r) \cdot \vec{n}_p\right) - \left(\vec{n}_{p_0} \times \vec{n}_p\right)\left(\vec{\nabla} g(r) \cdot \vec{J}\right)\right]\right\} ds_p = \vec{n}_{p_0} \times \vec{E}^0(P_0), \qquad (5)\\
&\oint\limits_S \left\{j\omega\mu_0 g(r)\left(\vec{n}_{p_0} \cdot \vec{J}\right) + \left(\vec{n}_{p_0} \cdot \vec{\nabla} g(r)\right) E_n(P)\right. \\
&\left. + W\vec{\nabla} g(r)\left(\left(\vec{n}_{p_0} \cdot \vec{J}\right)\vec{n}_p - \left(\vec{n}_{p_0} \cdot \vec{n}_p\right)\vec{J}\right)\right\} ds_p = \left(\vec{n}_{p_0} \cdot \vec{E}^0(P_0)\right). \qquad (6)
\end{aligned}$$

Solutions of SIE in Eqs. (5) and (6) have the form of equivalent current components that are excited at the surface S of impedance object by the incident field $\vec{E}^0$.

Next, we consider an example. The scattering object surface S will have the form of spherical screen. The most convenient coordinate system for this example is spherical.

Now, we find scalar products of Equation (5) with each of the unit vectors of spherical coordinate system $\vec{e}_{\rho_0}, \vec{e}_{\theta_0}, \vec{e}_{\varphi_0}$ at the observation point P_0. By doing this, we obtain three scalar integral equations:

$$\begin{aligned}
&\oint\limits_S \left\{j\omega\mu_0 g(r)\left(\vec{f}_1 \cdot \vec{J}\right) + \left(\vec{f}_1 \cdot \vec{\nabla} g(r)\right) E_n(P)\right. \\
&\left. + W\left[\left(\vec{f}_1 \cdot \vec{J}\right)\left(\vec{\nabla} g(r) \cdot \vec{n}_p\right) - \left(\vec{f}_1 \cdot \vec{n}_p\right)\left(\vec{\nabla} g(r) \cdot \vec{J}\right)\right]\right\} ds_p = \vec{f}_1 \cdot \vec{E}^0(P_0), \qquad (7)\\
&\oint\limits_S \left\{j\omega\mu_0 g(r)\left(\vec{f}_2 \cdot \vec{J}\right) + \left(\vec{f}_2 \cdot \vec{\nabla} g(r)\right) E_n(P)\right. \\
&\left. + W\left[\left(\vec{f}_2 \cdot \vec{J}\right)\left(\vec{\nabla} g(r) \cdot \vec{n}_p\right) - \left(\vec{f}_2 \cdot \vec{n}_p\right)\left(\vec{\nabla} g(r) \cdot \vec{J}\right)\right]\right\} ds_p = \vec{f}_2 \cdot \vec{E}^0(P_0), \qquad (8)\\
&\oint\limits_S \left\{j\omega\mu_0 g(r)\left(\vec{f}_3 \cdot \vec{J}\right) + \left(\vec{f}_3 \cdot \vec{\nabla} g(r)\right) E_n(P)\right. \\
&\left. + W\left[\left(\vec{f}_3 \cdot \vec{J}\right)\left(\vec{\nabla} g(r) \cdot \vec{n}_p\right) - \left(\vec{f}_3 \cdot \vec{n}_p\right)\left(\vec{\nabla} g(r) \cdot \vec{J}\right)\right]\right\} ds_p = \vec{f}_3 \cdot \vec{E}^0(P_0), \qquad (9)
\end{aligned}$$

were $\vec{f}_1 = \vec{e}_{\theta_0} \times \vec{n}_{p_0}$; $\vec{f}_2 = \vec{e}_{\varphi_0} \times \vec{n}_{p_0}$; $\vec{f}_3 = \vec{e}_{\rho_0} \times \vec{n}_{p_0}$.

Taken together with Eq. (6), these equations make up the system of scalar integral equations with respect to the sought-for currents at the screen's surface S.

Let's consider the screen generated by intersection of the spherical metallic screen of thickness h and internal radius a, with the right circular cylinder, its radius being b, and its axis of symmetry coinciding with axis Oz (see Fig. 2).

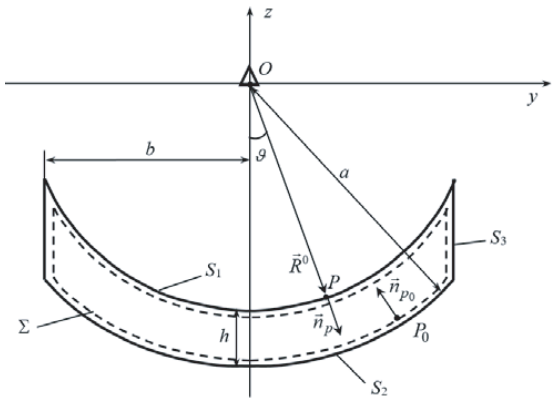

Figure 2. Axial cross-section of the antenna.

Let's break down the surface of spherical screen in the following form: $S = S_1 \cup S_2 \cup S_3$ (see Fig. 2).

Now, the surface current density $\vec{J}$ at the screen's surface S shall be found as sum:

$$\vec{J} = J_\theta^i(\theta,\varphi)\,\vec{e}_\theta + J_\varphi^i(\theta,\varphi)\,\vec{e}_\varphi \text{ at } S_i \ (i=1,2), \tag{10}$$

$$\vec{J} = J_z^3(z,\varphi)\,\vec{e}_z + J_\varphi^3(z,\varphi)\,\vec{e}_\varphi \text{ at } S_3, \tag{11}$$

where $\vec{e}_\theta = (-\cos\theta\cos\varphi, -\cos\theta\sin\varphi, -\sin\theta)$; $\vec{e}_z = (0,0,1)$; $\vec{e}_\varphi = (-\sin\varphi,\ \cos\varphi, 0)$.

Here $\vec{e}_\theta$, $\vec{e}_\varphi$ are orthogonal unit vectors of the spherical coordinate system at surfaces S_i $(i=1,2)$, and $\vec{e}_z$, $\vec{e}_\varphi$ are orthogonal unit vectors of the cylindrical coordinate system at surface S_3.

Next, we introduce the piecewise constant approximation of components of the surface current $\vec{J}$ at the screen's surface S. To do this, we break the surfaces S_m down into N_m areas S_{mj}, each having constant surface current density: $S_m = \sum\limits_{j=1}^{N_m} S_{mj}$ $(m=1,2,3)$.

Having done the latter approximation, we get the system of linear algebraic equations (SLAE) with respect to components of surface current density $J_{\theta j}^m$, $J_{\varphi j}^m$, J_{zj}^m over the areas S_{mj} of constant current densities. Coefficients of this SLAE are calculated as double integrals of smooth functions, which are computed as in [24]. Besides, the computational errors were controlled by comparing the integration results given various numbers of integration intervals in the Gauss compound formula. The integration error was kept below 0.2%.

The SLAE mentioned above was solved by the co-location method. The surface current density components found by solving the SLAE were used later for computing the field scattered by the screen at point M using Equation (1).

3. VERIFICATION OF COMPUTATIONAL METHOD

The computational method was verified by cross-checking the values of the radar cross-section (RCS) σ [27] obtained for the spherical screen against the corresponding measured values presented in [14]. For the convenience of cross-checking, we substituted the plane electromagnetic wave into the equation system of Eqs. (6)–(9). This plane wave has the following form:

$$\vec{E}^0\left(\vec{X}\right) = \vec{p}^{\,0} e^{jk_0\left(\vec{R}^0\cdot\vec{X}\right)}, \tag{12}$$

where $\vec{p}^0$ is the unit vector of the incident wave polarization; $\vec{R}^0$ is the unit vector of incidence direction; $\vec{X}$ is the radius vector of observation point.

Besides, results of computations by our method were also cross-checked against the data obtained for the perfectly conducting screen of zero thickness by Vinogradov [6].

Work [14] presents experimental RCS measurements for the aluminum spherical screen probed along its axis. The measurements were carried out for monochromatic illumination signals, whose frequency ranged from 26.2 GHz through 38.4 GHz, and the latter transforms into the values of k_0b from 6.89 through 10.12. The specimen under study had the following geometrical parameters: radius of spherical screen was $a = 18.08$ mm; radius of spherical screen's aperture was $b = 12.55$ mm; screen's thickness $h = 0.15$ mm.

The measurement of interest corresponded to the millimeter wavelength range. Our computations indicated that in this particular range of values k_0b, RCS of the screen strongly depends on the shape of its edge. The screens for the experiment in [14] were made manually; therefore, it was difficult to maintain the exact shape of the screen's edge according to variants 1 or 2 (as shown in Fig. 3) since the screen itself was quite small. Taking the latter into account, we have conducted two rounds of computations for two extreme cases corresponding to the two shapes of the screen's edge, and we had to present the results for both these cases. Besides, we assumed that specific conductance of aluminum was equal to 3.54×10^7 Sm/m.

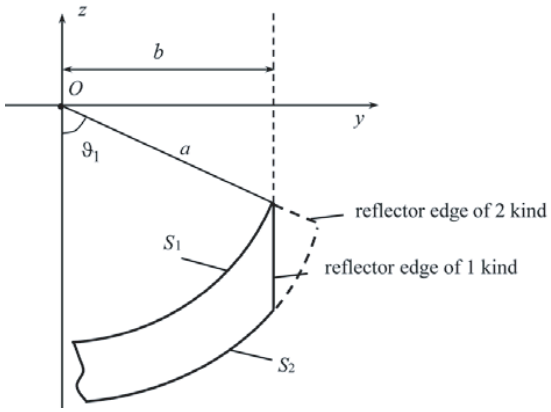

Figure 3. Shapes of the screen's edge.

Figure 4 presents the normalized RCS $\frac{\sigma}{\pi b^2}$ computed using our method together with the measured data given this particular spherical screen, whose features were specified above. The same figure presents the computed RCS of the zero thickness screen of perfect conductivity [6] (curve 4).

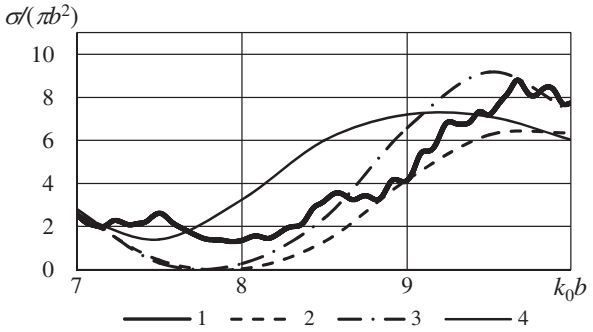

Figure 4. Normalized RCS of spherical screen versus k_0b (1 — measurement data [14]; 2 – results of computation given aluminum screen with the reflector's edge of first kind; 3 — results of computation given aluminum screen with the reflectors edge of second kind; 4 — results of computation given perfectly conducting screen of zero thickness [6]).

From Fig. 4, one can see that most part of experimental measurement curve is confined between the computed curves 2 and 3. Some differences given smaller values of $\frac{\sigma}{\pi b^2}$ ($7.25 < k_0 b < 8.25$) are due to manufacturing inaccuracy of the spherical screens used in the experiment, due to measurement errors, and due to the influence of auxiliary elements used to fix the screens onto the value of field scattered by the screen in [14].

We notice that the curve corresponding to the perfectly conducting screen of zero thickness [6] (curve 4 in Fig. 4) differs significantly from both measured and computed scattering data given the screen of non-zero thickness and non-perfect conductivity.

Method for solving the system of Equations (5), (7)–(9) is not different in principle from the numerical method for computing the field scattered from the perfectly conducting screens of zero thickness presented in [15]. Therefore, for simplicity sake, we present here the comparison of computations pertaining to the scattering of plane wave from the perfectly conducting disk of thickness $h = 0.05\lambda$. Fig. 5 shows the RCS versus illumination frequency given that disk was probed along its axis. RCS values were computed using numerical implementation of the method described in the paper (curve 1) and using the "Altair Feko" solver [28], the latter employing the method of moments (curve 2). The same plot presents the RCS computed using the physical optics (PO) method (curve 3).

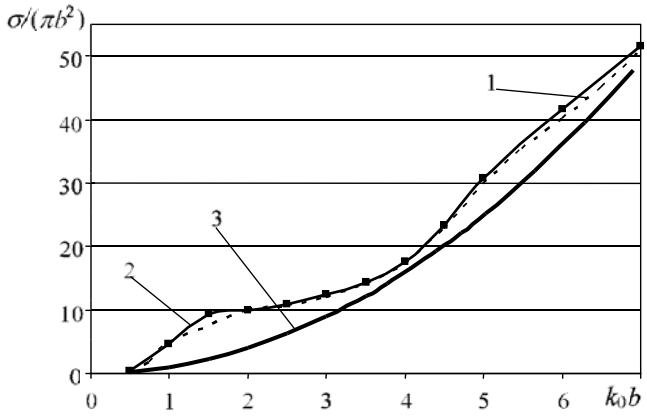

Figure 5. Computed RCS of the disk of thickness equal to 0.05λ (1 — the E-field integral equation solution, 2 — "Altair Feko" solution, 3 — physical optics solution).

It should be noted that the RCS curve computed using the PO method differs significantly from the first two curves. Curves 1 and 2 are pretty close to each other, which can be considered as certain verification of the method proposed here.

However, employment of the "Altair Feko" for significantly thinner screens can be problematic.

Works [25, 26] present the RCSs computed for spherical screens given $k_0 b$ ranging from 1 to 6, $1 < k_0 b < 6$ as compared with the case of perfectly conducting screens of zero thickness. It is this comparison that indicated the need for taking into account the actual conductivity and thickness of screens in the frequency range of interest.

4. COMPUTATION OF SIGNAL RADIATED BY ANTENNA WITH ALUMINUM SPHERICAL REFLECTOR

Below, we consider an example of employing our method to computing the radiation characteristics of reflector antennas with regard to ultra-wideband pulsed signals in time domain. We consider a reflector antenna with an aluminum reflector that has finite conductivity of 3.54×10^7 Sm/m. Geometric characteristics of the antenna were as follows: $b = 0.19$ m; $a = 0.269$ m; $h = 1$ mm. Antenna feed was placed at point O, Fig. 2.

We used a model source of ultra-wideband signal as the antenna feed, its radiation pattern for a spectrum component at the wavelength λ_0 being described by the field radiated by elementary Huygens

source [1, 29]:

$$E_{\theta}^{0}(P) = \frac{g(R)}{\lambda_0}(1+\cos\theta)\cos\varphi, \tag{13}$$

$$E_{\varphi}^{0}(P) = \frac{g(R)}{\lambda_0}(1+\cos\theta)\sin\varphi, \tag{14}$$

where R is the distance between the source and the point P at the reflector's surface (Fig. 2).

We considered antenna radiation ranging from 500 MHz through 1 GHz, which corresponded to the range of $2 < k_0 b < 4$. Signals with such a bandwidth belong to the class of ultra-wideband ones (the ratio of spectrum width to central spectrum frequency, also known as the index of bandwidth, was equal to 0.67).

Figure 6 shows the computed antenna directivity patterns (DP) $F(\theta)$ with respect to the radiated field in the plane yOz given a set of discrete frequencies within the range specified above. All DPs in Fig. 6 were normalized to the DP maximum at the radiation frequency of 1 GHz.

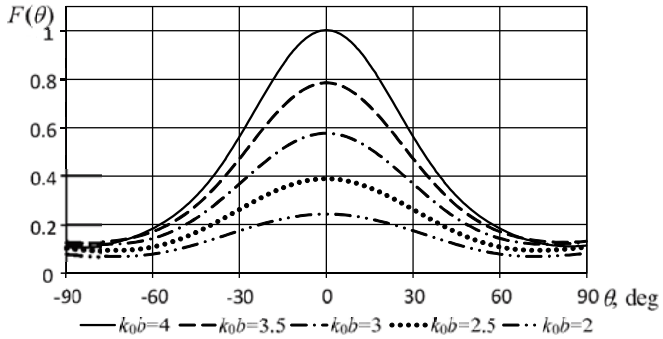

Figure 6. Normalized directivity patterns of antenna given various frequencies of the feed radiation.

Analysis of curves in Fig. 6 shows that individual DPs at fixed frequencies strongly depend on the frequency. In time domain, the latter translates into the waveform, whose shape depends on the radiation direction. Besides, the latter means that one cannot apply traditional concept of DP by field to the ultra-wideband signals.

Directional properties of an antenna with regard to transmission (reception) of UWB signals can be comprehensively described by the space-frequency dependence of its radiated (received) electric field component $\vec{E}(\omega, \vec{r})$ (or magnetic field component $\vec{H}(\omega, \vec{r})$). Here, $\vec{r}$ is the radius-vector of an observation point, and ω is the circular frequency. In contrast to antennas radiating monochromatic (narrowband) signals, for which ω is constant, the UWB antennas are characterized by functional dependence of the radiated field $\vec{E}(\omega, \vec{r})$ on the frequency $\omega_1 \leq \omega \leq \omega_2$ for every point in space $\vec{r}$. This dependence determines the shape of pulse radiated by reflector antenna in different directions.

We find it more convenient to work with space-time dependence of field $\vec{\mathcal{E}}(t, \vec{r})$, when dealing with UWB signals. The latter characteristic is related to the space-frequency one via the inverse Fourier transform:

$$\vec{\mathcal{E}}(t, \vec{r}) = \int_{\omega_1}^{\omega_2} \vec{E}(\omega, \vec{r})\, e^{-j\omega t} d\omega. \tag{15}$$

In our computations, we used the analog of Equation (15) with respect to wavenumber k_0:

$$\vec{\mathcal{E}}(ct, \theta) = \int_{k_1}^{k_2} \vec{E}(k_0, \theta)\, e^{-jk_0 ct} dk_0, \tag{16}$$

where c is the speed of light; k_1 and k_2 are the wavenumbers that correspond to the boundaries of signal's spectrum range.

So, we have computed the field radiated by antenna for a given set of discrete values of $k_0 b$ within the range of $2 < k_0 b < 4$ spaced by the value of 0.03125 (like those in Fig. 6). We also repeated these computations given various radiation directions θ. In this manner, we have obtained frequency responses of antenna given various radiation directions θ.

Next, we applied the inverse Fourier transform (16) to these frequency responses to obtain the signal waveforms in time domain given various values of θ. Fig. 7 shows the normalized radiated field amplitude $A/|A_0|_{\max}$ versus value of ct. There are two parts to it. Fig. 7(a) presents the waveform that illuminates the antenna reflector (maximum of the field radiated by the antenna feed being aligned with the reflector's center), and Fig. 7(b) presents the waveform radiated by the antenna in axial direction $\theta = 0°$.

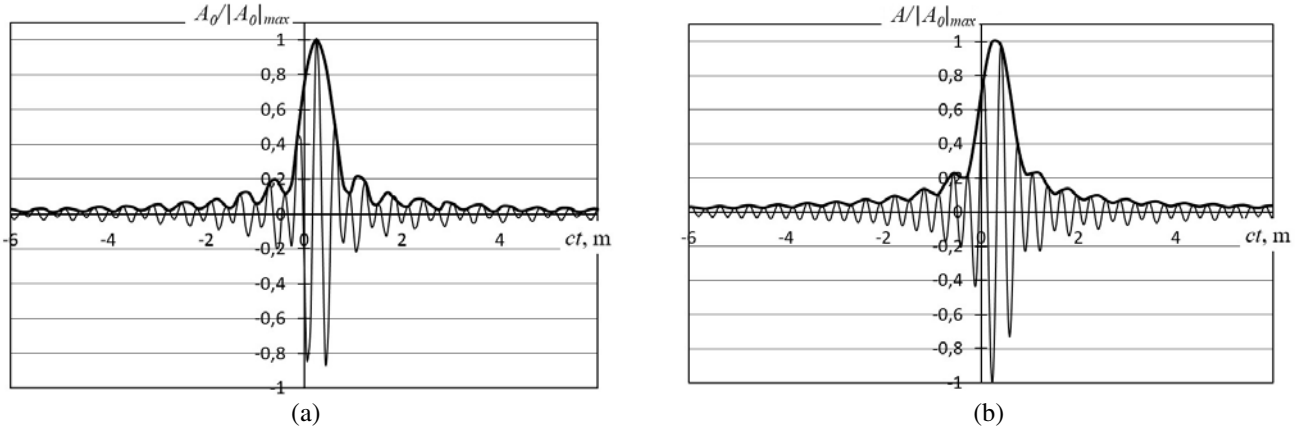

Figure 7. Signal waveform radiated by the antenna: (a) the waveform radiated by the feed towards the center of reflector; (b) the waveform radiated by the antenna in axial direction.

Bold lines in Fig. 7 correspond to the signal envelope. Comparison of Figs. 7(a) and 7(b) shows that after bouncing from the reflector the pulse radiated by the feed stretches up in time. In the example above, the duration of pulse radiated by antenna is greater by 7% than that of pulse illuminating the reflector as measured by the half-amplitude signal level. Besides, the signal envelope stretch is accompanied with its notches getting occluded.

From the standpoint of antenna directivity, which strictly speaking cannot be any longer described using the DP concept as long as the UWB signal is concerned, and it is convenient to consider the envelopes of the said UWB signal radiated in different directions.

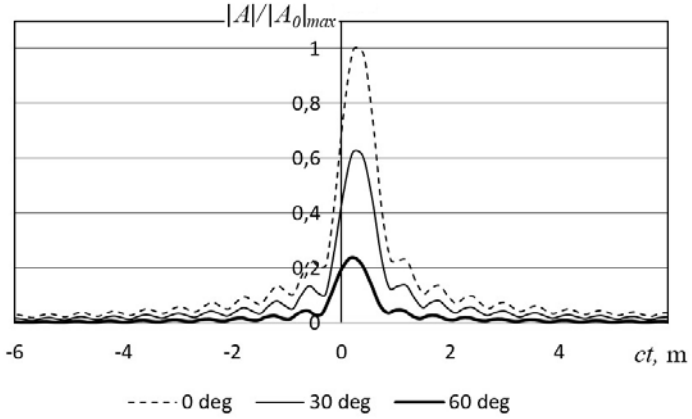

Figure 8. Envelopes of signals radiated in the directions $\theta = 0°$, 30°, and 60°.

So, we need to figure out the shape of signal radiated by antenna in directions other than the axial one. Fig. 8 presents the computed signal envelopes $|A|/|A_0|_{\max}$ radiated by the antenna in the directions of $\theta = 0°$, $30°$, and $60°$. All the envelopes are normalized with respect to the maximum signal magnitude that corresponds to the axial radiation direction.

Finally, the results shown in Fig. 8 characterize directivity properties of the antenna at hand. It is obvious from the plots that the peak radiation in the direction of $\theta = 30°$ drops to 0.62 with respect to that in the axial direction, and given the radiation direction of $\theta = 60°$, this peak drops to 0.24 with respect to that in the axial direction.

5. CONCLUSION

The article presents the method developed by the authors for computing scattering characteristics of well (but not perfectly) conducting screens of finite thickness (thin but not zero thin).

Comparison of RCSs obtained by rigorous computation with RCSs obtained by measurement as well as by computation under a simplifying assumption of infinitely thin and perfectly conducting screens indicated that in the resonant scattering region (screen sizes getting into the range $7 < k_0 b < 9$) there is considerable difference between these RCSs. Therefore, there is the necessity of accounting for the screen thickness and conductivity of the material that the screen is made of.

An example of using the method to evaluate the space-time characteristics of UWB signal radiation by a reflector antenna with a spherical reflector in the resonant frequency range was given. As a model of a UWB antenna feed, an idealized signal source was used, its spectral components being described by the field radiated by elementary Huygens element. The method allows to evaluate the distortion of the UWB signal introduced by its scattering from an antenna. The method proposed here can be used for computing the radiation properties of antennas with reflectors, whose shapes differ from spherical ones (for example, parabolic, elliptical, cylindrical, and others).

REFERENCES

1. Milligan, T. A., *Modern Antenna Design*, 2nd edition, John Wiley & Sons, Inc., Hoboken, New Jersey, 2005.
2. Povzner, A. Y. and I. V. Sukharevsky, "Second kind integral equations for diffraction problems on the infinitely thin screen," *Doklady Sovetskoy Physiki*, Vol. 4, 798–801, 1960.
3. Feld, Y. N. and I. V. Sukharevsky, "On the integral equations of diffraction problems on unclosed screens," *Radioteknika I Elektronika*, Vol. 12, No. 10, 1713–1720, 1967 (in Russian).
4. Ilyinsky, A. S. and Y. G. Smirnov, "Electromagnetic wave diffraction by conducting screens," Utrecht, Ridderprint, Netherlands, 1998.
5. Smirnov, Y. G., "The solvability of vector integro-differential equations for the problem of the diffraction of an electromagnetic fields by screens of arbitrary shape," *Comp. Meths. Math. Phys.*, Vol. 34, No. 10, 1265–1276, 1994.
6. Vinogradov, S. S., P. D. Smith, and E. D. Vinogradova, *Canonical Problems in Scattering and Potential Theory. Part 2: Acoustic and Electromagnetic Diffraction by Canonical Structures*, Chapman & Hall/CRC, 2002.
7. Vinogradov, S. S., Y. A. Tuchkin, and V. P. Shestopalov, "On the theory of the scattering of waves by nonclosed screens of spherical shape," *Soviet Physics Doklady*, Vol. 26, No. 2, 169–171, 1981.
8. Davydov, A. G., Y. V. Zaharov, and Y. V. Pimenov, "Method of numerical solution of electromagnetic diffraction problem on arbitrary unclosed surfaces," *Doklady Akademii Nauk SSSR*, Vol. 276, No. 1, 96–100, 1984 (in Russian).
9. Bulygin, V. S., A. I. Nosich, and Y. V. Gandel, "Nystrom-type method in three-dimensional electromagnetic diffraction by a finite PEC rotationally symmetric surface," *IEEE Trans. Antennas Propagat.*, Vol. 60, No. 10, 4710–4718, 2012.
10. Sukharevsky, O. I., "Electrodynamic calculation of a model of the two-mirror antenna with exact account of interaction between mirrors," *Radiotekhnika*, Vol. 60, 41–47, 1982.

11. Rao, S. M., D. R. Wilton, and A. W. Glisson, "Electromagnetic scattering by surfaces of arbitrary shape," *IEEE Trans. Antennas Propagat.*, Vol. 30, No. 5, 409–418, 1982.
12. James, R. M., "On the use of F.S./F.F.T.'s as global basis functions in the solution of boundary integral equations for EM scattering," *IEEE Trans. Antennas Propagat.*, Vol. 42, No. 9, 213–219, 1994.
13. Trowbridge, B., "Integral equations in electromagnetics," *Intern. J. Numerical Modeling: Electronic Networks, Devices and Fields*, Vol. 9, No. 3, 978–984, 1996.
14. Ivanchenko, D. D. and I. O. Sukharevsky, "Backscattering measurements for metallic unclosed spherical screens," *Telecommunications and Radio Engineering*, Vol. 69, No. 5, 423–428, 2010.
15. Sukharevsky, I. O., G. S. Zalevsky, S. V. Nechitaylo, and O. I. Sukharevsky, "Electromagnetic wave scattering by a circular perfectly conducting disc of finite thickness," *Electromagnetic Waves and Electronic Systems*, Vol. 15, No. 2, 42–47, 2010 (in Russian).
16. Sukharevsky, I. O., S. V. Nechitaylo, D. D. Ivanchenko, and P. N. Melezhik, "Electromagnetic wave scattering by a curved screen of finite thickness," *Telecommunications and Radio Engineering*, Vol. 71, No. 5, 413–422, 2012.
17. Kyurkchan, A. G. and N. I. Smirnova, "Solution of wave diffraction problems by the null-field method," *Acoustical Physics*, Vol. 55, No. 6, 691–697, 2009.
18. Wriedt, T., "Review of null-field method with discrete sources," *Journal of Quantitative Spectroscopy & Radiative Transfer*, Vol. 106, 535–545, 2007.
19. Stratton, J. A., *Electromagnetic Theory*, McGraw-Hill, New-York, 1941.
20. Silver, S., *Microwave Antenna Theory and Design, MIT Radiation Laboratory Series*, Vol. 12, McGraw-Hill, New York, 1949.
21. Yuferev, S. V. and N. Ida, *Surface Impedance Boundary Conditions: A Comprehensive Approach*, CRC Press, 2010.
22. Colton, D. and R. Kress, "Integral equation methods in scattering theory," *(SIAM-Society for Industrial and Applied Mathematics*, 2013.
23. Waterman, P. C., "Matrix formulation of electromagnetic scattering," *Proc. IEEE*, Vol. 53, 805–812, 1965.
24. Bakhvalov, N. S., N. P. Zhidkov, and G. M. Kobelnikov, *Numerical Methods: Teaching Aid*, Nauka, Moscow, 1987.
25. Nechitaylo, S., V. Orlenko, O. Sukharevsky, and V. Vasylets, "Electromagnetic wave scattering by a screen of finite thickness and conductivity," *Telecommunications and Radio Engineering*, Vol. 77, No. 16, 1409–1421, 2018.
26. Sukharevsky, O., S. Nechitaylo, V. Orlenko, and V. Vasylets, "Frequency response of impedance screens of finite thickness in the resonance band," *Proc 9th Int Conf on Ultrawideband and Ultrashort Impulse Signals*, 28–33, Odessa, Ukraine, September 2018.
27. Sukharevsky, O. I., et al., *Electromagnetic Wave Scattering by Aerial and Ground Radar Objects*, O. I. Sukharevsky (ed.), CRC Press, 2014.
28. https://altairhyperworks.com/product/FEKO.
29. Fang, D. G., *Antenna Theory and Microstrip Antennas*, CRC Press, 2010.